Chemical Geology 522 (2019) 186–191

Contents lists available at ScienceDirect

Chemical Geology

journal homepage: www.elsevier.com/locate/chemgeo

Combined high-precision Δ_{48} and Δ_{47} analysis of carbonates

Jens Fiebig[a,*], David Bajnai[a], Niklas Löffler[b], Katharina Methner[b], Emilija Krsnik[b], Andreas Mulch[a,b], Sven Hofmann[a]

[a] Institute of Geosciences, Goethe University, Altenhöferallee 1, 60438 Frankfurt am Main, Germany
[b] Senckenberg Biodiversity and Climate Research Center, Senckenberganlage 25, 60325 Frankfurt am Main, Germany

ARTICLE INFO

Editor: Jérôme Gaillardet

Keywords:
Clumped isotopes
Carbonates
Δ_{47}
Δ_{48}
Paleotemperatures
Biomineralization

ABSTRACT

High-precision analysis of the excess abundance (relative to the stochastic distribution) of mass 48 isotopologues in CO_2 evolved from acid digestion of carbonates (Δ_{48}) has not been possible until recently due to the relatively low natural abundance of ^{18}O. Here we show that the 253 Plus™ gas source mass spectrometer equipped with Faraday cups and 10^{13} Ω resistors can perform combined Δ_{47} and Δ_{48} analyses on carbonates with external reproducibilities (1SD) of 0.010 ‰ and 0.030 ‰, respectively.

~10 mg aliquots of five carbonate reference materials (ETH 1, ETH 2, ETH 3, ETH 4, and Carrara) are digested with phosphoric acid at 90 °C using a common acid bath. The evolved CO_2 is purified using an automated gas preparation system (including cryotraps and a GC) and analyzed for its Δ_{47} and Δ_{48} compositions using the dual inlet system of a 253 Plus™ gas source mass spectrometer. Raw Δ_{47} and Δ_{48} values are finally normalized to the Carbon Dioxide Equilibrium Scale (CDES).

In Δ_{47}, $_{CDES\ 90°C}$ *vs.* Δ_{48}, $_{CDES\ 90°C}$ space, calcite reference materials Carrara, ETH 3 and ETH 4 agree with the equilibrium curve for calcite after adding semi-empirically determined 90 °C acid fractionation factors of 0.196 ‰ (for Δ_{47}) and 0.136 ‰ (for Δ_{48}) to theoretical Δ_{63} and Δ_{64} data. Agreement between measured and theoretically expected Δ_{48}, $_{CDES\ 90°C}$ highlights the accuracy of our high-precision clumped isotope analytical setup. Combined analysis of the abundances of mass 47 and mass 48 isotopologues in CO_2 evolved from acid digestion of natural carbonates has excellent potential for the determination of accurate and highly precise paleotemperatures as well as for the identification of rate-limiting kinetic processes involved in biomineralization. A formation temperature of 15(± 2) °C is obtained on the 95 % confidence level for the Upper Cretaceous chalk sample ETH 3.

1. Introduction

Clumped isotope analysis of the sum of $^{13}C^{18}O^{16}O$ and $^{12}C^{18}O^{17}O$ isotopologues (Δ_{47}) in CO_2 evolved from phosphoric acid digestion of carbonates (Ghosh et al., 2006) has become a now increasingly utilized (paleo)thermometer (Eiler, 2011) to determine marine (*e.g.*, Wierzbowski et al., 2018) and terrestrial (*e.g.*, Methner et al., 2016) paleotemperatures, body temperatures of extinct vertebrates (*e.g.*, Eagle et al., 2011), diagenetic (*e.g.*, Huntington et al., 2011) and hydrothermal temperatures (*e.g.*, Bristow et al., 2011) as well as closure temperatures of metamorphic rocks (*e.g.*, Passey and Henkes, 2012). Since this type of thermometer is based on the internal fractionation of isotopes amongst carbonate isotopologues, it is independent on the isotopic composition of the water from which the carbonate-bearing phase precipitated. Nonetheless, discrepant Δ_{47}–temperature calibrations have been obtained in different laboratories (Dennis and Schrag, 2010; Ghosh et al., 2006; Fernandez et al., 2017; Petersen et al., 2019). Accuracy of Δ_{47} calibration data has been shown to be sensitive to the choice of parameters used for the correction of (1) contributions deriving from ^{17}O-bearing CO_2 (Daëron et al., 2016; Schauer et al., 2016), (2) pressure baseline effect (Bernasconi et al., 2013; Fiebig et al., 2016; He et al., 2012), (3) scale compression (Dennis et al., 2011; Huntington et al., 2009), and (4) acid fractionation (Petersen et al., 2019). Also, calibration regression lines can be biased if the number of samples and replicates per sample, as well as the investigated temperature range, is relatively low (Fernandez et al., 2017). The observed discrepancy in Δ_{47}–T calibrations is slightly reduced if calibration data from eight experimental and six empirical studies are processed with the IUPAC ^{17}O parameters, recommended by Daëron et al. (2016), and with a unique temperature dependence of the acid fractionation factor (Petersen et al., 2019). However, even for these reprocessed calibrations the absolute spread in Δ_{47} at a given temperature remains as large

* Corresponding author.
E-mail address: Jens.Fiebig@em.uni-frankfurt.de (J. Fiebig).

https://doi.org/10.1016/j.chemgeo.2019.05.019
Received 11 February 2019; Received in revised form 9 May 2019; Accepted 14 May 2019
Available online 25 May 2019

as 0.08 ‰, with slopes ranging from 0.033 to 0.042 in Δ_{47} *vs.* $1/T^2$ space (Petersen et al., 2019). Most recent investigations suggest that much of the observed scatter could be due to kinetics occurring in the solution prior to carbonate precipitation and at the solution-carbonate interface (Bajnai et al., 2018; Daëron et al., 2019). If relevant, kinetic departures from equilibrium would limit the accuracy of the clumped isotope Δ_{47} paleothermometer.

The second most abundant carbonate isotopologue containing two heavy isotopes is $^{12}C^{18}O^{18}O^{16}O$. CO_2 derived from acid digestion of carbonate contains on average 4.1 ppm of $^{12}C^{18}O^{18}O$ (mass 48), which is an order of magnitude lower than its $^{13}C^{18}O^{16}O$ (mass 47) content (Ghosh et al., 2006). Another mass 48 isotopologue is $^{13}C^{18}O^{17}O$ that has an average natural abundance of 16.7 ppb only. The weighted sum of the excess abundances of mass 48 isotopologues (relative to their stochastic distributions) is reflected by the Δ_{48} value:

$$\Delta_{48} = [(R_{48}/R_{48}^{*} - 1) - 2 \times (R_{46}/R_{46}^{*} - 1)] \times 1000 \quad (1)$$

where Ri and Ri* represent the measured and stochastic* i/44 isotopologue ratios.

Like Δ_{47}, the carbonate Δ_{48} composition does not depend on the oxygen isotopic composition of the water from which the carbonate crystallized. The position of a given carbonate sample in Δ_{47} *vs.* Δ_{48} space is, therefore, determined by its formation temperature and, if kinetics prevailed during formation, by the extent of kinetic departure from equilibrium. Since kinetically induced departures from equilibrium follow for given rate-limiting exchange mechanisms characteristic trajectories in Δ_{47} *vs.* Δ_{48} space, it should be possible to determine accurate carbonate formation temperatures based on measured Δ_{47} and Δ_{48} compositions even if these were affected by kinetics (Guo and Zhou, 2019).

So far, the precision of Δ_{48} measurements with common gas source mass spectrometers equipped with $\leq 10^{12}$ Ω amplifiers has been inadequate to permit temperature estimates based on Δ_{48}. Instead, laboratories that analyze Δ_{48} use its magnitude for data quality assurance of Δ_{47} data, *i.e.*, as an indicator of potential isobaric interferences on *m/z* 47 (Huntington et al., 2009). Here we demonstrate that high-precision Δ_{47} and Δ_{48} analyses of carbonates are possible using a common acid bath and the dual inlet of a Thermo Scientific™ 253 Plus™ gas source mass spectrometer. The external reproducibilities for these measurements are close to the predicted shot noise limits. Our results imply that internal isotopic equilibrium is closely attained in calcite reference materials ETH 1, ETH 2, ETH 3, ETH 4, and Carrara.

2. Experimental

2.1. Samples

Calcite reference materials analyzed for this study were an in-house Carrara and the internationally distributed ETH 1, ETH 2, ETH 3, and ETH 4 standards (Bernasconi et al., 2018). ETH 1 (Carrara marble) and ETH 2 (synthetic high-purity calcite) were internally equilibrated at 600 °C. ETH 3 represents Upper Cretaceous chalk from the Isle of Rügen, Germany, whereas ETH 4 is the synthetic high-purity calcite that was also used for the preparation of ETH 2. The formation temperatures of ETH 3 and ETH 4 calcites are unknown (Meckler et al., 2014; Bernasconi et al., 2018). Bernasconi et al. (2018) reported $\Delta_{47, \text{CDES 25 °C}}$ for ETH 1, ETH 2, ETH 3 and ETH 4 that were assigned using the dual inlet system for equilibrated gas measurements and a Thermo Scientific™ KIEL IV Carbonate Device for carbonate-derived CO_2 measurements.

2.2. Carbonate reaction and gas purification

The setup of the self-constructed automated carbonate acid digestion and gas purification system (Hofmann's Auto Line, HAL) used for sample preparation is displayed in Fig. 1. It consists of a Zero Blank Autosampler (Costech Analytical Technologies, USA), a common acid bath, several cryotraps and a gas chromatograph (GC; 2.0 m of 1/8″ stainless steel tube packed with Porapak™ Q 80–100 mesh, Merck, Germany) and two turbopumps (HiCube 80 Eco, Pfeiffer Vacuum, Germany) with cryogenic water traps upstream of the turbo pumps. One pumps the part of the extraction line in front of the GC, including the autosampler and the common acid bath, the other provides the high vacuum for the two cryotraps in front of and behind the GC. Per replicate, ~10 mg of calcite is loaded into silver capsules (IVA Analysentechnik, Germany). These are then placed into the autosampler, located on top of the common acid bath. Once loading is completed, the autosampler and the common acid bath are turbo-pumped for at least 5 h. Slight rotation of the autosampler forces a sample-bearing silver capsule to drop down into the phosphoric acid (> 105 wt%). Carbonate samples are routinely reacted for 30 min, and the evolving CO_2 is continuously removed at −196 °C in trap 2. Trap 1 is kept at −80 °C to remove water. During the reaction, the pressure is continuously monitored at trap 2. After the reaction is complete, traps 2, 3 and 4 are set to −80 °C, while trap 5 is cooled to −196 °C. Helium (purity > 5.0; Alphagaz™ He, Air Liquide, France, gas led through a Supelco® 27600-U, Merck, Germany, helium purifier) enters trap 2 at a flow rate of 15 ml/min and purges the CO_2 through trap 3, the GC column (kept at −15 °C) and trap 4, before it is frozen out again in trap 5. After 45 min, the GC column is purged with He in the reverse flow, heated to 150 °C and kept at this temperature until the next sample is being prepared. Helium is pumped away from trap 5. Afterwards, trap 5 is warmed up to −80 °C and trap 6 cooled down to −196 °C. The yield of CO_2 is determined in the volume of trap 5 and the CO_2 then frozen out in trap 6. Once freezing is complete, trap 6 is isolated from trap 5, warmed up to −80 °C and the pure CO_2 introduced into the sample bellow of the mass spectrometer through expansion. HAL is controlled with the software LabVIEW (National Instruments, USA).

2.3. Equilibrated gases and gas purification

CO_2, equilibrated at 1000 °C for at least 2 h in a quartz break seal tube (GM Associates, USA), is taken off the muffle furnace and quenched to room temperature within 2 min. The break seal tube is mounted on a tube cracker that is connected to a high vacuum (water trap upstream the turbopump), manually operated gas extraction line. Within < 5 min after having left the muffle furnace, the break seal tube is cracked, and the CO_2 is passed twice over a water trap kept at −80 °C. The CO_2 is finally quantitatively transferred into a quartz glass with a pneumatic diaphragm valve (Swagelok, USA) at its top ("autofinger"). The same high vacuum line is used to clean CO_2 equilibrated at 25 °C and to transfer it to the autofinger. However, before CO_2 equilibrated at 25 °C is allowed to enter the manually operated high-vacuum gas purification line, liquid water is stripped off on a separate, rotary vane-pumped gas extraction line by passing the CO_2 five times over a cryogenic water trap kept at −80 °C. This way we can avoid that any significant amounts of water enter the high-vacuum gas preparation line.

The autofinger is finally connected to HAL in front of trap 2 (Fig. 1). There, equilibrated gases follow the same preparation pathway as carbonate-derived CO_2 with the exception that they enter HAL isolated from the common acid bath. Equilibrated gases are prepared in amounts equivalent to the CO_2 derived from carbonates (between 80 and 100 μmol).

2.4. Mass spectrometric measurements

Isotopic analyses are carried out on a Thermo Scientific™ 253 Plus™ (Thermo Fisher Scientific, Germany) gas source mass spectrometer using its dual inlet system. The 253 Plus™ at the Goethe University has Faraday cups for *m/z* 44, 45, 46, 47, 47.5, 48 and 49. Cups for *m/z* 44–46 have 3×10^8 Ω, 3×10^{10} Ω, and 10^{11} Ω resistors, respectively, while *m/z* 47–49 cups are amplified by 10^{13} Ω resistors. The m/z 47.5

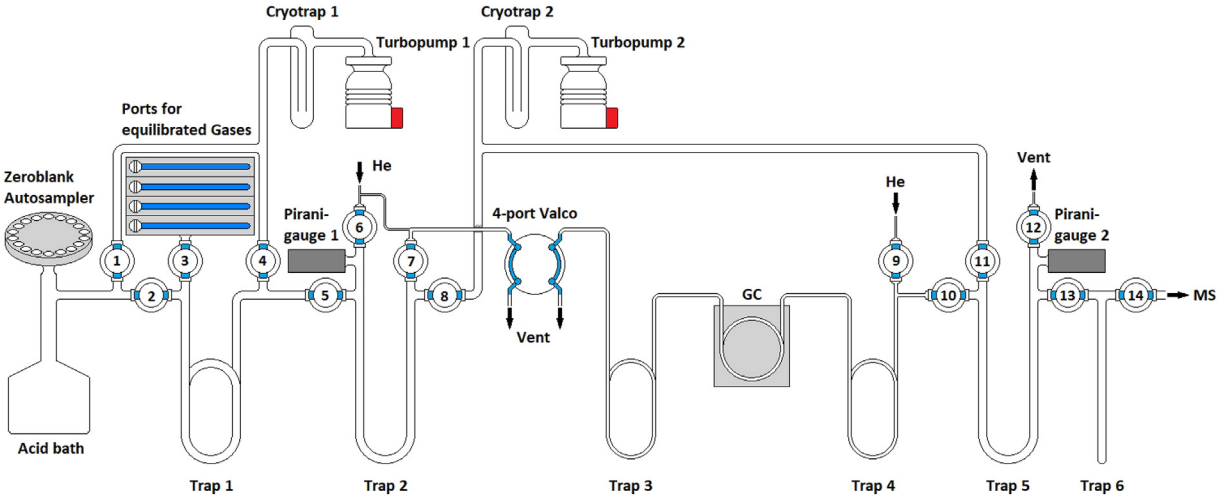

Fig. 1. Schematic setup of Hofmann's Auto Line (HAL). For more detailed explanation see text.

cup is used to continuously read in the pressure baseline next to m/z 47.

After the sample bellow has been loaded with CO_2, an equivalent amount (80–100 μmol) of reference gas CO_2 (ISO-TOP, Air Liquide; $\delta^{18}O_{VSMOW} = 25.26$ ‰, $\delta^{13}C_{VPDB} = -4.20$ ‰) is introduced into the reference gas bellow. Reference and sample gas enter the ion source of the 253 Plus™ gas source mass spectrometer through stainless steel capillaries whose inner surface is coated with inert fused silica (Thermo Fisher Scientific; bre 00014684). Reference and sample gas intensity are automatically adjusted to an intensity of 16,000(± 100) mV on m/z 44. Sample and reference gas are measured in 10 acquisitions, consisting of 10 cycles each. Each cycle considers an integration time of 20 s both for the reference and the sample gas, yielding a total integration time of 2000 s per replicate. Idle time is set to 16 s.

2.5. Data processing

The common background correction with no gas in the source is not applied. The negative background that is read in on *m/z* 47.5 is directly added to the raw intensities obtained for m/z 47, m/z 48 and m/z 49 in Isodat using a scaling factor of -1. Acquisition files are then exported to Easotope (release 20190125) (John and Bowen, 2016) which performs the calculation of $\delta^{13}C_{VPDB}$, $\delta^{18}O_{VSMOW}$, δ_{47}, δ_{48}, $\Delta_{47,\ raw}$ and $\Delta_{48,\ raw}$ using the IUPAC parameters (Daëron et al., 2016).

3. Results

A total of 76 carbonate reference samples and 38 equilibrated gases were run within a period of 8 weeks in January and February 2019. $\delta^{13}C_{VPDB}$, $\delta^{18}O_{VSMOW}$, δ_{47}, δ_{48}, $\Delta_{47,\ raw}$ and $\Delta_{48,\ raw}$ of equilibrated gases and carbonate reference materials are listed in Supplementary Data. For

Table 1

$\Delta_{47,\ CDES\ 90°C}$ and $\Delta_{48,\ CDES\ 90°C}$ of carbonate reference materials analyzed in this study. All values are processed using the IUPAC parameters recommended by Daëron et al. (2016) and are reported in ‰-deviation relative to the stochastic distribution. 1 SD and 2 SE denote the 1 σ standard deviation and the 2 σ standard error, respectively. The shot noise limit represents the best analytical precision that can be obtained. It was calculated from Eq. (15) of Merrit and Hayes (1994), considering the total integration time represented by the total number of replicates (2000 s × number of replicates).

	Carrara		ETH 4		ETH 3		ETH 2		ETH 1	
	$\Delta_{47,\ CDES\ 90°C}$	$\Delta_{48,\ CDES\ 90°C}$	$\Delta_{47,\ CDES\ 90°C}$	$\Delta_{48,\ CDES\ 90°C}$	$\Delta_{47,\ CDES\ 90°C}$	$\Delta_{48,\ CDES\ 90°C}$	$\Delta_{47,\ CDES\ 90°C}$	$\Delta_{48,\ CDES\ 90°C}$	$\Delta_{47,\ CDES\ 90°C}$	$\Delta_{48,\ CDES\ 90°C}$
	0.312	0.173	0.462	0.263	0.623	0.305	0.226	0.171	0.220	0.093
	0.318	0.123	0.469	0.196	0.630	0.242	0.212	0.136	0.222	0.132
	0.312	0.103	0.464	0.167	0.611	0.285	0.213	0.123	0.216	0.158
	0.319	0.172	0.456	0.227	0.615	0.296	0.214	0.151	0.203	0.159
	0.317	0.127	0.437	0.205	0.629	0.255	0.200	0.119	0.193	0.138
	0.307	0.144	0.447	0.218	0.628	0.212	0.223	0.195	0.201	0.181
	0.307	0.125	0.455	0.240	0.602	0.289	0.203	0.129	0.213	0.106
	0.303	0.111	0.455	0.249	0.627	0.260	0.207	0.135	0.218	0.115
	0.316	0.126	0.462	0.238	0.630	0.208	0.202	0.167	0.211	0.107
	0.314	0.141	0.458	0.258	0.614	0.252	0.205	0.089	0.208	0.094
	0.310	0.106	0.457	0.194	0.616	0.277	0.206	0.168	0.200	0.143
	0.335	0.229			0.609	0.285	0.212	0.147	0.215	0.116
					0.613	0.286	0.210	0.138	0.228	0.134
					0.630	0.304	0.235	0.121	0.216	0.129
					0.623	0.237	0.222	0.137	0.223	0.133
					0.611	0.321	0.227	0.125	0.220	0.121
							0.230	0.082	0.215	0.220
							0.221	0.156	0.224	0.174
									0.222	0.175
Average	0.314	0.140	0.457	0.223	0.619	0.270	0.215	0.138	0.214	0.138
1 SD	0.008	0.036	0.009	0.030	0.009	0.033	0.011	0.028	0.009	0.033
2 SE	0.005	0.023	0.006	0.020	0.005	0.018	0.005	0.014	0.005	0.016
Shot noise limit	0.002	0.008	0.002	0.008	0.002	0.007	0.002	0.006	0.002	0.006

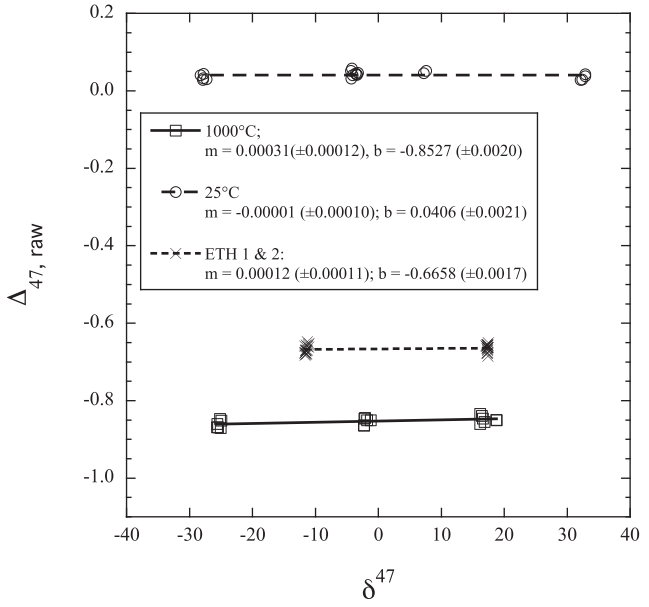

Fig. 2. Plot of $\Delta_{47,\ raw}$ *vs.* δ_{47} for CO_2 equilibrated at 1000 °C and 25 °C, respectively, as well as for carbonate reference materials ETH 1 and ETH 2. $\Delta_{47,\ raw}$ and δ_{47} values are relative to the working gas composition. Slopes (m) and intercepts (b) of the corresponding regression lines, as well as their errors, are provided for further information.

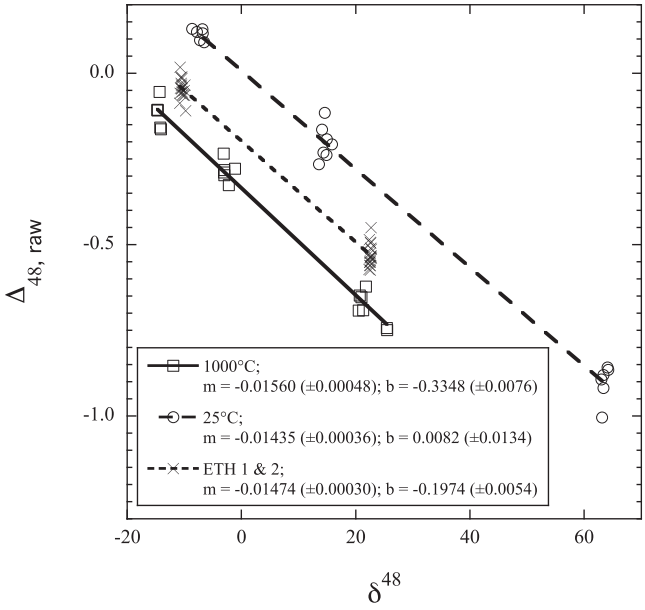

Fig. 3. Plot of $\Delta_{48,\ raw}$ *vs.* δ_{48} for CO_2 equilibrated at 1000 °C and 25 °C, respectively, as well as for carbonate reference materials ETH 1 and ETH 2. $\Delta_{48,\ raw}$ and δ_{48} values are relative to the working gas composition. Slopes (m) and intercepts (b) of the corresponding linear regression lines, as well as their errors, are provided for further information.

the carbonate reference materials, we also present a summary table in which measured $\Delta_{47,\ raw}$ and $\Delta_{48,\ raw}$ values were finally projected onto the carbon dioxide equilibrium scale (CDES) (Table 1).

4. Discussion

4.1. Background correction

Fig. 2 displays the correlation between δ_{47} and $\Delta_{47,\ raw}$ for CO_2 equilibrated at 1000 °C and 25 °C, respectively, as well as for ETH 1 and ETH 2. The slopes of the corresponding regression lines are almost zero, demonstrating that the *m/z* 47.5 cup accurately reads in the negative background below m/z 47. However, since there is a slight residual slope for the heated gases that is distinguishable from zero, an additional slope correction of $\Delta_{47,\ raw}$ data needs to be applied (Huntington et al., 2009). To determine this slope, 1000 °C and 25 °C gas data are merged, adding the average difference between the two corresponding regression lines to the heated gas $\Delta_{47,\ raw}$ values. This way, a residual slope of 0.00012 (± 0.00008) is obtained that exactly matches the residual slope displayed by ETH 1 and ETH 2 raw data (Fig. 2). Slope corrected $\Delta_{47,\ sc}$ values are calculated according to Eq. (2):

$$\Delta_{47,sc} = \Delta_{47,raw} - (m_{47} \times \delta_{47}) \quad (2)$$

where m_{47} is the residual slope, in our case 0.00012.

Correlation plots of δ_{48} *vs.* $\Delta_{48,\ raw}$, however, yield significant steeper residual negative slopes (Fig. 3). In addition, the slopes vary slightly between −0.01435(± 0.00036) for 25 °C gases, −0.01474(± 0.00030) for ETH 1 and ETH 2 and − 0.01560(± 0.00048) for heated gases. These residual slopes result from an overcorrection of the negative background occurring below *m/z* 48 when using the intensity monitored by the m/z 47.5 cup. The merged data set of equilibrated gases is characterized by a slope of −0.01479(± 0.00027), which is indistinguishable from the slope displayed by ETH 1 and ETH 2 data. As was done for slope correction of $\Delta_{47,\ raw}$ data, we, therefore, use the slope obtained from the ETH 1 and ETH 2 data (Fig. 3) to correct all sample $\Delta_{48,\ raw}$ data for the overcorrection induced by the m/z 47.5 intensity:

$$\Delta_{48,sc} = \Delta_{48,raw} - (m_{48} \times \delta_{48}) \quad (3)$$

where m_{48} is the residual slope, in this study −0.01474.

4.2. Projecting $\Delta_{47,\ sc}$ and $\Delta_{48,\ sc}$ sample values to the carbon dioxide equilibrium scale

Empirical transfer functions for the projection of $\Delta_{47,\ sc}$ and $\Delta_{48,\ sc}$ sample values onto the CDES can be derived following the principles outlined in Dennis et al. (2011), by plotting $\Delta_{47,\ sc}$ and $\Delta_{48,\ sc}$ values of equilibrated gases against their corresponding theoretical values. $\Delta_{47,\ sc}$ and $\Delta_{48,\ sc}$ values of equilibrated gases are reflected by the intercepts of equilibrated gas data regression lines in $\Delta_{47,\ raw}$ *vs.* δ_{47} space (Fig. 2) and $\Delta_{48,\ raw}$ *vs.* δ_{48} space (Fig. 3), respectively. Theoretical $\Delta_{48,\ 1000°C}$ and $\Delta_{48,\ 25°C}$ values are not directly available but can be computed from the data provided by Wang et al. (2004), who calculated the temperature dependence of $\Delta_{12C18O18O}$ and $\Delta_{13C18O17O}$ as a function of temperature. Considering that $^{12}C^{18}O^{18}O$ contributes 99.6 % and $^{13}C^{18}O^{17}O$ 0.4 % to m/z 48, theoretical Δ_{48} values at any temperature can be computed according to:

$$\Delta_{48,CO2} = 0.996 \times \Delta_{12C18O18O} + 0.004 \times \Delta_{13C18O17O} \quad (4)$$

After processing the data of Wang et al. (2004) (their Table 4(I)) through Eq. (4), a best fit polynomial regression yields:

$$\Delta_{48,CO2} = -1.0345 \times 10^{-4} \times (10^6/T^2)^3 + 4.22629 \times 10^{-3} \times (10^6/T^2)^2 - 3.76112 \times 10^{-3} \times (10^6/T^2) \quad (5)$$

According to Eq. (5), the theoretical Δ_{48} should be 0.345 ‰ and 0.000 ‰ for CO_2 at temperatures of 25 °C and 1000 °C, respectively. At these temperatures, the corresponding theoretical Δ_{47} values are 0.9252 ‰ and 0.0266 ‰, respectively (Dennis et al., 2011).

In $\Delta_{47,\ raw}$ *vs.* δ_{47} space, the difference in intercepts between 1000 °C (−0.8527(± 0.0020)) ‰ and 25 °C CO_2 (0.0406(± 0.0021)) ‰ matches the theoretical difference of 0.90 ‰ (Fig. 2). This observation strongly implies that the 253 Plus™ installed at the joint Goethe University – Senckenberg BIK-F stable isotope facility is devoid of any significant scale compression for Δ_{47}, contrary to the MAT 253™ that was run in the same laboratory using electropolished nickel capillaries

(Fiebig et al., 2016). For the determination of $\Delta_{47,\ CDES\ 90°C}$ the following empirical transfer function is obtained:

$$\Delta_{47,\ CDES\ 90°C} = 1.0060 \times \Delta_{47,sc} + 0.8843 \quad (6)$$

In $\Delta_{48,\ raw}$ *vs.* δ_{48} space, intercepts of $-0.3348(\pm 0.0076)$ ‰ and $0.0082(\pm 0.0134)$ ‰ are obtained for CO_2 equilibrated at 1000 °C and 25 °C, respectively (Fig. 3). Again, the difference between the two intercepts is in perfect agreement with the theoretically expected value of 0.345‰. The hypothesis that the 253 Plus™ installed in our laboratory is not affected by any significant scale compression is, therefore, confirmed by Δ_{48} data of equilibrated gases. It follows:

$$\Delta_{48,\ CDES\ 90°C} = 1.0056 \times \Delta_{48,sc} + 0.3367 \quad (7)$$

$\Delta_{47,\ CDES\ 90°C}$ and $\Delta_{48,\ CDES\ 90°C}$ computed for carbonate reference materials ETH 1, ETH 2, ETH 3, ETH 4 and Carrara are listed in Table 1. For these, it becomes obvious that $\Delta_{48,\ CDES\ 90°C}$ increases with $\Delta_{47,\ CDES\ 90°C}$. Such behavior is expected if both compositions are largely controlled by temperature. External reproducibilities (expressed as 1 σ standard deviation, 1 SD) range from ± 0.008 ‰ to ± 0.011 ‰ for $\Delta_{47,\ CDES\ 90°C}$ and from ± 0.028 to ± 0.036 ‰ for $\Delta_{48,\ CDES\ 90°C}$ (Table 1). These values are only slightly higher than the predicted shot noise limits of 0.008 ‰ and 0.027 ‰, respectively, which represent the best attainable precision for the chosen analytical conditions of 2000 s integration time per replicate (Merrit and Hayes, 1994). Compared to the MAT 253™ (1SD of 11–16 ppm, see Fiebig et al. (2016)), the external reproducibility for dual inlet-based Δ_{47} measurements with the high-ohmic 253 Plus™ is improved by a factor of 1.5.

4.3. $\Delta_{47,\ CDES\ 25°C}$ values of ETH carbonate reference materials

Addition of a 25–90 °C acid fractionation factor of 0.088 ‰ (Petersen et al., 2019) to the $\Delta_{47,\ CDES\ 90°C}$ values reported in Table 1 yields $\Delta_{47,\ CDES\ 25°C}$ values (± 1 SD) of 0.302(± 0.009) ‰ for ETH 1, 0.303(± 0.011) ‰ for ETH 2, 0.707(± 0.009) ‰ for ETH 3, and 0.545(± 0.009) ‰ for ETH 4. These values are significantly different from those reported in Bernasconi et al. (2018), even if 0.004 ‰ are added to the latter data to account for the unique temperature dependence of the acid fractionation factor (note that Bernasconi et al. (2018) reacted at 70 °C and that a 25–70 °C acid fractionation of 0.062 ‰ was applied to their data, which slightly deviates from the 0.066 ‰ reported in Petersen et al., 2019). We speculate that the observed differences may arise from the circumstance that in the analytical setup used by Meckler et al. (2014) and Bernasconi et al. (2018) CO_2 gas derived from the ETH standards did not enter the ion source of the gas source mass spectrometer through the same stainless steel capillary as the equilibrated gases. If small amounts of water were adsorbed at the inner surface of the sample gas capillary, partial re-equilibration of CO_2 at ambient temperature may happen while the CO_2 passes through the capillary, finally introducing a compression of the Δ_{47}-scale. Partial re-equilibration may attain a steady state as long as the water content and the gas flux through the capillary are constant. Under such conditions, sample-derived CO_2 can still be accurately projected onto the CDES if the equilibrated gases enter the ion source through the same capillary as the sample gases. However, the same correction procedure may deliver inaccurate results if two different capillaries with distinct water contents and fluxes are used, as already stated by Bernasconi et al. (2018).

4.4. Comparing measured $\Delta_{47,\ CDES\ 90°C}$ and $\Delta_{48,\ CDES\ 90°C}$ with predicted equilibrium values

According to Hill et al. (2014), the B3LYP (6-311 + + G(2d,2p)) supramolecular cluster model describes the temperature dependence of equilibrium clumping in calcite most reliably. To make measured $\Delta_{47,\ CDES\ 90°C}$ and $\Delta_{48,\ CDES\ 90°C}$ comparable with equilibrium Δ_{63} and Δ_{64} values, the acid fractionation factors Δ^*_{47-63} and Δ^*_{48-64}, characteristic for a reaction at 90 °C, have to be added to the Δ_{63} and Δ_{64} values, respectively. These can be constrained from measured and theoretical data. For ETH 1 and ETH 2, we obtain mean $\Delta_{47,\ CDES\ 90°C}$ and $\Delta_{48,\ CDES\ 90°C}$ values of 0.214(± 0.010) ‰ and 0.138(± 0.030) ‰, respectively (Table 1). According to Hill et al. (2014), a Δ_{63} value of 0.018 ‰ and a Δ_{64} value of 0.002 ‰ is predicted for calcite at 600 °C, *i.e.*, the temperature at which ETH 1 and ETH 2 were prepared. Subtracting these values from the mean $\Delta_{47,\ CDES\ 90°C}$ and $\Delta_{48,\ CDES\ 90°C}$ values obtained for ETH 1 and ETH 2 yields Δ^*_{47-63} and Δ^*_{48-64} acid fractionation factors of 0.196 ‰ and 0.136 ‰, respectively. Theoretically expected $\Delta_{47,\ CDES\ 90°C}$ and $\Delta_{48,\ CDES\ 90°C}$ values for CO_2 derived from acid digestion of equilibrated calcite may now be computed adding Δ^*_{47-63} and Δ^*_{48-64} to the theoretical Δ_{63} and Δ_{64} values of Hill et al. (2014) at any temperature.

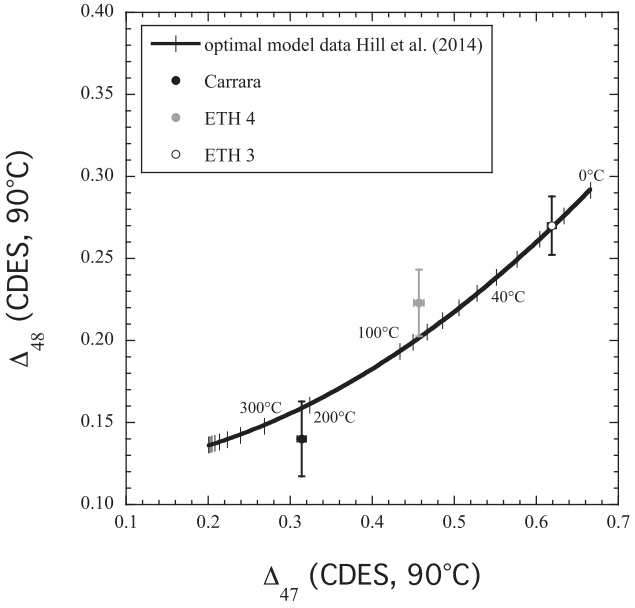

Fig. 4. Plot of $\Delta_{48,\ CDES\ 90°C}$ *vs.* $\Delta_{47,\ CDES\ 90°C}$ for ETH 3, ETH 4 and Carrara. Within errors (2 SE, 95 % confidence level), all data points agree with the theoretical equilibrium curve after adding the experimentally determined phosphoric acid fractionation factors of 0.136 ‰ and 0.196 ‰, respectively, to the theoretical Δ_{64} and Δ_{63} values for calcite (Hill et al., 2014).

Fig. 4 provides a comparison of theoretical equilibrium with measured values in $\Delta_{47,\ CDES\ 90°C}$ *vs.* $\Delta_{48,\ CDES\ 90°C}$ space. Generally, measured $\Delta_{48,\ CDES\ 90°C}$ for ETH 3, ETH 4 and Carrara confirm measured $\Delta_{47,\ CDES\ 90°C}$ values in that $\Delta_{48,\ CDES\ 90°C}$ increases with $\Delta_{47,\ CDES\ 90°C}$. This is expected if both $\Delta_{48,\ CDES\ 90°C}$ and $\Delta_{47,\ CDES\ 90°C}$ are primarily controlled by temperature. Moreover, within errors (2 SE, 95 % confidence level), measured $\Delta_{47,\ CDES\ 90°C}$ and $\Delta_{48,\ CDES\ 90°C}$ values agree with theoretical equilibrium implying that internal isotopic equilibrium may have been attained in all investigated carbonates. We would not expect such a systematic correlation between $\Delta_{47,\ CDES\ 90°C}$ and $\Delta_{48,\ CDES\ 90°C}$ for these three carbonates if isobaric interferences on *m/z* 47 and m/z 48 were of importance.

Should equilibrium really have been attained in ETH 3, ETH 4 and Carrara, it would have been established at temperatures of 15(± 2) °C, 86(± 4) °C, and 210(± 7) °C, respectively, as reflected from measured $\Delta_{47,\ CDES\ 90°C}$ values (Fig. 4). However, considering the error in $\Delta_{48,\ CDES\ 90°C}$, we alternatively cannot rule out that the true $\Delta_{47,\ CDES\ 90°C}$ and $\Delta_{48,\ CDES\ 90°C}$ compositions of Carrara and ETH 4 plot slightly below or above the equilibrium line, respectively (Fig. 4). Generally, departures from equilibrium would be introduced by rate-limiting kinetic effects. It has recently been shown that the most prominent rate-limiting processes involved in carbonate precipitation, CO_2 absorption and CO_2 degassing, follow specific trajectories in $\Delta_{47,\ CDES\ 90°C}$ *vs.* $\Delta_{48,\ CDES\ 90°C}$

space (Guo and Zhou, 2019). Hence, even if kinetics were of any importance during carbonate mineralization, it should be possible to determine accurate formation temperatures, along with the rate-limiting step governing isotopic exchange, solely based on the position of measured data in $\Delta_{47,\ CDES\ 90°C}$ *vs.* $\Delta_{48,\ CDES\ 90°C}$ space (Guo and Zhou, 2019).

5. Conclusions

We describe an analytical setup that allows accurate and precise determination of Δ_{48} along with Δ_{47} in CO_2 evolved from phosphoric acid digestion of carbonates. External reproducibilities for Δ_{48} and Δ_{47} analyses occur close to the corresponding shot-noise limits. There is no indication that the chosen setup introduces any significant artificial biases in the measured abundances of mass 47 and mass 48 CO_2 isotopologues.

Supplementary data to this article can be found online at https://doi.org/10.1016/j.chemgeo.2019.05.019.

Acknowledgments

We would like to thank Stefano Bernasconi for reviewing this paper. This work became possible through DFG grant INST 161/871-1.

References

Bajnai, D., Fiebig, J., Tomašových, A., Milner Garcia, S., Rollion-Bard, C., Raddatz, J., Löffler, N., Primo-Ramos, C., Brand, U., 2018. Assessing kinetic fractionation in brachiopod calcite using clumped isotopes. Sci. Rep. 8 (1), 1–12. https://doi.org/10.1038/s41598-017-17353-7.

Bernasconi, S.M., Hu, B., Wacker, U., Fiebig, J., Breitenbach, S.F., Rutz, T., 2013. Background effects on Faraday collectors in gas-source mass spectrometry and implications for clumped isotope measurements. Rapid Commun. Mass Spectrom. 27 (5), 603–612. https://doi.org/10.1002/rcm.6490.

Bernasconi, S.M., Müller, I.A., Bergmann, K.D., Breitenbach, S.F.M., Fernandez, A., Hodell, D.A., Jaggi, M., Meckler, A.N., Millan, I., Ziegler, M., 2018. Reducing uncertainties in carbonate clumped isotope analysis through consistent carbonate-based standardization. Geochem. Geophys. Geosyst. 19 (9), 2895–2914. https://doi.org/10.1029/2017gc007385.

Bristow, T.F., Bonifacie, M., Derkowski, A., Eiler, J.M., Grotzinger, J.P., 2011. A hydrothermal origin for isotopically anomalous cap dolostone cements from south China. Nature 474, 68–71. https://doi.org/10.1038/nature10096.

Daëron, M., Blamart, D., Peral, M., Affek, H.P., 2016. Absolute isotopic abundance ratios and the accuracy of Δ_{47} measurements. Chem. Geol. 442, 83–96. https://doi.org/10.1016/j.chemgeo.2016.08.014.

Daëron, M., Drysdale, R.N., Peral, M., Huyghe, D., Blamart, D., Coplen, T.B., Lartaud, F., Zanchetta, G., 2019. Most Earth-surface calcites precipitate out of isotopic equilibrium. Nat. Commun. 10 (429), 1–7. https://doi.org/10.1038/s41467-019-08336-5.

Dennis, K.J., Schrag, D.P., 2010. Clumped isotope thermometry of carbonatites as an indicator of diagenetic alteration. Geochim. Cosmochim. Acta 74 (14), 4110–4122. https://doi.org/10.1016/j.gca.2010.04.005.

Dennis, K.J., Affek, H.P., Passey, B.H., Schrag, D.P., Eiler, J.M., 2011. Defining an absolute reference frame for 'clumped' isotope studies of CO_2. Geochim. Cosmochim. Acta 75 (22), 7117–7131. https://doi.org/10.1016/j.gca.2011.09.025.

Eagle, R.A., Tütken, T., Martin, T.S., Tripati, A.K., Fricke, H.C., Connely, M., Cifelli, R.L., Eiler, J.M., 2011. Dinosaur body temperatures determined from isotopic (^{13}C-^{18}O) ordering in fossil biominerals. Science 333 (6041), 443–445. https://doi.org/10.1126/science.1206196.

Eiler, J.M., 2011. Paleoclimate reconstruction using carbonate clumped isotope thermometry. Quat. Sci. Rev. 30 (25–26), 3575–3588. https://doi.org/10.1016/j.quascirev.2011.09.001.

Fernandez, A., Müller, I.A., Rodríguez-Sanz, L., van Dijk, J., Looser, N., Bernasconi, S.M., 2017. A reassessment of the precision of carbonate clumped isotope measurements: implications for calibrations and paleoclimate reconstructions. Geochem. Geophys. Geosyst. 18, 1–12. https://doi.org/10.1002/2017gc007106.

Fiebig, J., Hofmann, S., Löffler, N., Lüdecke, T., Methner, K., Wacker, U., 2016. Slight pressure imbalances can affect accuracy and precision of dual inlet-based clumped isotope analysis. Isot. Environ. Health Stud. 52 (1–2), 12–28. https://doi.org/10.1080/10256016.2015.1010531.

Ghosh, P., Adkins, J., Affek, H., Balta, B., Guo, W., Schauble, E.A., Schrag, D., Eiler, J.M., 2006. ^{13}C–^{18}O bonds in carbonate minerals: a new kind of paleothermometer. Geochim. Cosmochim. Acta 70 (6), 1439–1456. https://doi.org/10.1016/j.gca.2005.11.014.

Guo, W., Zhou, C., 2019. Δ_{48} fractionation in carbonates and its implications for clumped isotope thermometry. In: Paper Presented at the 7th International Clumped Isotope Workshop, Queen Mary, Long Beach, CA, USA.

He, B., Olack, G.A., Colman, A.S., 2012. Pressure baseline correction and high-precision CO_2 clumped-isotope (Δ_{47}) measurements in bellows and micro-volume modes. Rapid Commun. Mass Spectrom. 26 (24), 2837–2853. https://doi.org/10.1002/rcm.6436.

Hill, P.S., Tripati, A.K., Schauble, E.A., 2014. Theoretical constraints on the effects of pH, salinity, and temperature on clumped isotope signatures of dissolved inorganic carbon species and precipitating carbonate minerals. Geochim. Cosmochim. Acta 125, 610–652. https://doi.org/10.1016/j.gca.2013.06.018.

Huntington, K.W., Eiler, J.M., Affek, H.P., Guo, W., Bonifacie, M., Yeung, L.Y., Thiagarajan, N., Passey, B., Tripati, A., Daeron, M., Came, R., 2009. Methods and limitations of 'clumped' CO_2 isotope (Δ_{47}) analysis by gas-source isotope ratio mass spectrometry. J. Mass Spectrom. 44 (9), 1318–1329. https://doi.org/10.1002/jms.1614.

Huntington, K.W., Budd, D.A., Wernicke, B.W., Eiler, J.M., 2011. Use of clumped isotope thermometry to constrain the crystallization temperature of diagenetic calcite. J. Sediment. Res. 81, 656–669. https://doi.org/10.2110/jsr.2011.51.

John, C.M., Bowen, D., 2016. Community software for challenging isotope analysis: first applications of 'Easotope' to clumped isotopes. Rapid Commun. Mass Spectrom. 30 (21), 2285–2300. https://doi.org/10.1002/rcm.7720.

Meckler, A.N., Ziegler, M., Millan, M.I., Breitenbach, S.F., Bernasconi, S.M., 2014. Long-term performance of the KIEL Carbonate Device with a new correction scheme for clumped isotope measurements. Rapid Commun. Mass Spectrom. 28 (15), 1705–1715. https://doi.org/10.1002/rcm.6949.

Merrit, D.A., Hayes, J.M., 1994. Factors controlling precision and accuracy in isotope-ratio-monitoring mass spectrometry. Anal. Chem. 66, 2336–2347. https://doi.org/10.1021/ac00086a020.

Methner, K., Mulch, A., Fiebig, J., Wacker, U., Gerdes, A., Graham, S.A., Chamberlain, C.P., 2016. Rapid Middle Eocene temperature change in western North America. Earth Planet. Sci. Lett. 450, 132–139. https://doi.org/10.1016/j.epsl.2016.05.053.

Passey, B.H., Henkes, G.A., 2012. Carbonate clumped isotope bond reordering and geospeedometry. Earth Planet. Sci. Lett. 351-352, 223–236. https://doi.org/10.1016/j.epsl.2012.07.021.

Petersen, S.V., Defliese, W.F., Saenger, C., Daëron, M., Huntington, K.W., John, C.M., Kelson, J.R., Coleman, A.S., Kluge, T., Olack, G.A., Schauer, A.J., Bajnai, D., Bonifacie, M., Breitenbach, S.F., Fiebig, J., Fernandez, A.B., Henkes, G.A., Hodell, D., Katz, A., Kele, S., Lohmann, K.C., Passey, B.H., Peral, M.Y., Petrizzo, D.A., Rosenheim, B.E., Tripati, A., Venturelli, R., Young, E.D., Winkelstern, I.Z., 2019. Effects of improved ^{17}O correction on inter-laboratory agreement in clumped isotope calibrations, estimates of mineral-specific offsets, and acid fractionation factor temperature dependence. Geochem. Geophys. Geosyst. https://doi.org/10.1029/2018GC008127. (in press).

Schauer, A.J., Kelson, J., Saenger, C., Huntington, K.W., 2016. Choice of ^{17}O correction affects clumped isotope (Δ_{47}) values of CO_2 measured with mass spectrometry. Rapid Commun. Mass Spectrom. 30 (24), 2607–2616. https://doi.org/10.1002/rcm.7743.

Wang, Z., Schauble, E.A., Eiler, J.M., 2004. Equilibrium thermodynamics of multiply substituted isotopologues of molecular gases. Geochim. Cosmochim. Acta 68 (23), 4779–4797. https://doi.org/10.1016/j.gca.2004.05.039.

Wierzbowski, H., Bajnai, D., Wacker, U., Rogov, M.A., Fiebig, J., Tesakova, E.M., 2018. Clumped isotope record of salinity variations in the Subboreal Province at the middle–late Jurassic transition. Glob. Planet. Chang. 167, 172–189. https://doi.org/10.1016/j.gloplacha.2018.05.014.